A novel upper bound finite-element for the limit analysis of plates and shells

Jeremy Bleyer[a,*]

[a]*Laboratoire Navier, ENPC, Univ Gustave Eiffel, CNRS, Marne-la-vallée, France*

Abstract

Shear-locking is a classical issue in displacement-based finite-element approaches for thick plates and shells. It is even more important when considering kinematic limit analysis approaches which attempt at producing an upper bound estimate of the structure collapse load. Previous locking-free finite-element discretizations for thick plates either rely on mixed approaches or approximate strain compatibility relations which inevitably loose the upper bound status of the solution or on discontinuous interpolations which are difficult to implement and have a much higher computational cost. In this contribution, we investigate the use of a simple element with a continuous quadratic displacement and a piecewise linear rotation with continuity at the element mid-edges only. We show that this element can either produce strict upper-bound estimates taking into account the contribution of rotation jumps or a pseudo-upper bound when neglecting this contribution. Although the upper bound status is lost a priori in this case, numerical evidence indicate that limit loads usually converge from above and have a very good accuracy. Finally, we also use this element for shell problems and discuss in particular the formulation of strength criteria for thick shells. Illustrative applications show that the proposed element is free from any shear locking and produces very accurate limit load estimates for plate as well as shell problems.

Keywords: limit analysis, yield design, thick plates, thick shells, shear-locking, conic programming

[*]*Correspondence to*: J. Bleyer, Laboratoire Navier, 6-8 av Blaise Pascal, Cité Descartes, 77455 Champs-sur-Marne, France, Tel : +33 (0)1 64 15 37 43, Email: `jeremy.bleyer@enpc.fr`

1. Introduction

Limit analysis [24] (or yield design theory [44, 45] in a more general framework) is a direct approach enabling to compute the ultimate load of a structure under the sole requirements of equilibrium on one hand and strength conditions on the other hand. The satisfaction of these two conditions is at the basis of the so-called lower bound static approach. The upper bound kinematic approach is the corresponding dual formulation when writing the virtual work principle for any potential collapse mechanism. The material strength criterion is a convex set in the stress space and is represented through its support function in terms of the strain rate associated with some collapse mechanism.

Numerical resolution of limit analysis problems usually rely on the finite-element method [2, 34, 42]. The corresponding discrete problem is however cast into a convex maximization (for the lower bound approach) or minimization problem (for the upper bound approach). State-of-the-art methods for solving the corresponding optimization problems are interior-point solvers for conic programming [26, 41]. The use of such techniques require the material strength conditions to be written using conic constraints [5, 13, 35]. Fortunately, most common strength criteria can be formulated in such a manner, see for instance [11] for the specific case of shells. Finally, we can also mention strain-driven approaches using a path-following strategy and standard closest-point return mappings which can be interpreted as proximal optimization procedures [21, 22].

As regards discretization strategies, the lower bound static approach relies on equilibrium-based finite-elements [27, 47]. The upper bound kinematic approach can be used either with standard continuous displacement-based interpolations or discontinuous interpolations [28, 36–38, 48]. Despite a higher computational cost compared to equivalent continuous interpolations, discontinuous interpolations provide more accurate limit load estimates [28, 37, 42, 48].

Discretizations for the upper-bound limit analysis of plates in bending are more challenging. Indeed, it is known that C^1-continuity is required for classical analysis of thin plates which is hard to enforce using simple finite-elements [16, 30]. Rotation discontinuities must therefore be accounted

for to use simpler elements achieving only C^0-continuity for the deflection [9, 12, 25]. Similarly for thick plates, C^1-continuity is relaxed but the use of continuous interpolations for the deflection and rotation will inevitably lead to shear-locking in the thin plate limit [14]. Different techniques can be proposed to alleviate shear-locking including selective reduced integration [51], mixed formulation/hybrid elements [17, 23, 32], enhanced assumed strain [46], discrete shear gap elements [29], etc. For all these method, the upper bound status is inevitably lost and their implementation is not always easy. In [14], it is shown that fully discontinuous interpolations are naturally free from any shear-locking and preserve the upper bound status by accounting for the discontinuities contribution.

As regards shells, problems are similar with the additional issue of membrane locking and the absence of drilling rotation stiffness in most formulations. Works considering limit analysis problems with shell models have been mainly analytical for simple cases with only scarce works devoted to numerical aspects for generic shells [4, 11, 13, 39, 49].

The manuscript is organized as follows: section 2 describes the proposed finite-element discretization in the case of thick plates, section 3 is devoted to its application to shell structures, illustrative applications are considered in section 4 and section 5 concludes this work.

The numerical implementations of the present work have been performed by following the automated limit analysis formulation framework described in [13]. This framework is based on the `fenics_optim` package [8], see also [7], which relies on the `FEniCS` finite-element software package [1, 33] and the `Mosek` conic programming solver [40].

Notations. Vectors are denoted with lower case bold symbols and 2nd-rank tensors with upper case bold symbols. $\mathrm{sym}(\star) = (\star + \star^{\mathrm{T}})/2$ is the symmetry operator, $\nabla^s \star = \mathrm{sym}(\nabla \star)$ denotes the symmetrized gradient operator and $\boldsymbol{u} \overset{s}{\otimes} \boldsymbol{v} = \mathrm{sym}(\boldsymbol{u} \otimes \boldsymbol{v})$ the symmetrized outer product. $[\![\star]\!]$ the discontinuity of a field across some discontinuity line of unit normal $\boldsymbol{n}$. $\boldsymbol{u} \times \boldsymbol{v}$ denotes the cross product between two 3D vectors. We also extend the notation to the cross-product between a vector and a 2nd-rank tensor as follows: $\boldsymbol{u} \times \boldsymbol{A} = \boldsymbol{u} \times (A_{ij} \boldsymbol{e}_i \otimes \boldsymbol{e}_j) = A_{ij} (\boldsymbol{u} \times \boldsymbol{e}_i) \otimes \boldsymbol{e}_j$, and similarly for $\boldsymbol{A} \times \boldsymbol{u}$.

2. A new upper bound discretization for thick plates

2.1. Upper bound kinematic limit analysis of thick plates

Let us recall the upper bound kinematic formulation of limit analysis for thick plates, the notation will essentially follow that of [13]. Ω denotes the plate mid-surface, lying in the $(\boldsymbol{e}_x, \boldsymbol{e}_y)$ plane with $\boldsymbol{e}_z$ being the plate transverse direction. Strength conditions for thick plates involve both the bending moment tensor $\boldsymbol{M} = \begin{bmatrix} M_{xx} & M_{xy} \\ M_{xy} & M_{yy} \end{bmatrix}$ and the shear force vector $\boldsymbol{Q} = (Q_x, Q_y)$. In [10, 14], different choices of thick plate criteria are discussed, especially regarding the bending/shear interaction. We will denote by G such a generic thick plate strength criterion i.e. $(\boldsymbol{M}, \boldsymbol{Q}) \in G$.

The kinematic formulation relies on a Reissner-Mindlin kinematics involving an out-of-plane deflection w and an in-plane rotation vector $\boldsymbol{\theta} = (\theta_x, \theta_y)$. Let us consider a distributed vertical loading of reference intensity $f(\boldsymbol{x})$. We aim at computing the corresponding limit load $\lambda^+ f(\boldsymbol{x})$ where λ^+ denotes the ultimate load factor associated with the structure collapse. Following [14], the upper-bound limit analysis problem can be written as:

$$\begin{aligned} \lambda^+ \leq \lambda_k = \inf_{w,\boldsymbol{\theta}} \quad & \int_\Omega \pi_G(\nabla^s \boldsymbol{\beta}, \nabla w - \boldsymbol{\beta}) \,\mathrm{dx} + \int_\Gamma \Pi_G([\![\boldsymbol{\beta}]\!], [\![w]\!]; \boldsymbol{n}) \,\mathrm{dS} \\ \text{s.t.} \quad & \int_\Omega f w \,\mathrm{dx} = 1 \end{aligned} \tag{1}$$

where $\boldsymbol{\beta} = \boldsymbol{e}_z \times \boldsymbol{\theta}$ and where the following support functions have been introduced:

$$\pi_G(\boldsymbol{\chi}, \boldsymbol{\gamma}) = \sup_{(\boldsymbol{M},\boldsymbol{Q}) \in G} \{\boldsymbol{M} : \boldsymbol{\chi} + \boldsymbol{Q} : \boldsymbol{\gamma}\} \tag{2}$$

$$\Pi_G([\![\boldsymbol{\beta}]\!], [\![w]\!]; \boldsymbol{n}) = \sup_{(\boldsymbol{M},\boldsymbol{Q}) \in G} \{(\boldsymbol{M} \cdot \boldsymbol{n}) \cdot [\![\boldsymbol{\beta}]\!] + (\boldsymbol{Q} \cdot \boldsymbol{n}) [\![w]\!]\} \tag{3}$$

where $\boldsymbol{\chi} = \nabla^s \boldsymbol{\beta}$ is the curvature and $\boldsymbol{\gamma} = \nabla w - \boldsymbol{\beta}$ the shear strain. In (1), the last term of the objective involves the contribution of potential discontinuities of the rotation $[\![\boldsymbol{\beta}]\!]$ and of the deflection $[\![w]\!]$ to the upper-bound collapse load estimate λ_k. Taking into account such discontinuities contributions preserves the upper-bound status of the computed limit load estimate. In this regard, a finite-element discretization in limit analysis can consider discontinuous interpolations for the deflection and the rotation field.

As previously mentioned, considering a continuous interpolation for both w and $\boldsymbol{\theta}$ will result in shear-locking in the thin plate limit, except if specific procedures are undertaken which inevitably destroy the upper bound status of the computed estimate. Shear-locking can be simply alleviated by considering a discontinuous interpolation for both variables as in [14] where w is assumed to be piecewise quadratic and $\boldsymbol{\theta}$ piecewise linear. In this case, both the curvature and the shear strain are piecewise linear. As discussed in [13, 36], the first term in (1) objective can be computed by excess using a numerical quadrature with three integration points located at the element vertices (the so-called *vertex* scheme). A specific approximation of the integral should be used to also approximate by excess the second term of (1) due to the quadratic variation of $[\![w]\!]$ along each finite-element edge, see for instance [37]. However, it must be noted that such contributions are usually quite small, especially with mesh refinement, and vanish in the thin plate limit. The impact on the upper bound status is usually quite negligible.

2.2. The proposed element

In order to reduce the computational cost associated with the use of fully discontinuous interpolations, we consider now the following choice:

- w is assumed to be continuous and quadratic (6-node triangle)
- $\boldsymbol{\theta}$ is assumed to be linear on each element with continuity ensured only at the mid-edges of each element. This interpolation is known as the Crouzeix-Raviart element in the mathematical community where it has first been introduced in [20] as a non-conforming discretization for the stationary Stokes problem.

The proposed choice has already been considered by [15] for a non-linear shell model. Interestingly, this element did not deserve much attention in the literature despite its good performance, see for instance [6] for its use with elastic thick plates[1]. Its main advantage is that this element is naturally free from any-shear locking without resorting to any stabilizing techniques such as reduced integration, mixed methods or assumed strains. Note that Crouzeix-Raviart elements have already been used in Reissner-Mindlin plate

[1] `https://comet-fenics.readthedocs.io/en/latest/demo/reissner_mindlin_crouzeix_raviart/reissner_mindlin_CR.html`

models such as in [3] but on the deflection field rather than the rotation.

With the present choice, curvature and shear strain are still piecewise linear, the deflection jump is zero and the rotation jump $[\![\boldsymbol{\beta}]\!]$ is linear over each edge (it is null at the edge midpoint). As a result, the contribution of rotation discontinuities can now be approximated by excess with two integration points located at the edge vertices. The resulting discrete formulation of (1) is therefore given by:

$$\lambda^+ \leq \lambda_{\mathrm{UB}} = \min_{\boldsymbol{U}} \sum_{e \in \texttt{elements}} \frac{A_e}{3} \sum_{i=1}^{3} \pi_G(\boldsymbol{\chi}_i, \boldsymbol{\gamma}_i) + \sum_{j \in \texttt{edges}} \frac{\ell_j}{2} \sum_{i'=1}^{2} \Pi_G([\![\boldsymbol{\beta}]\!]_{i'}, 0; \boldsymbol{n}_j) \quad \text{s.t.} \quad \boldsymbol{F}^{\mathrm{T}}\boldsymbol{U} = 1 \tag{4}$$

where $\boldsymbol{U}$ (resp. $\boldsymbol{F}$) is the global vector of degrees of freedom (resp. nodal forces), A_e the area of a current element e, χ_i (resp. γ_i) the value of the curvature (resp. shear strain) at vertex i of this element, ℓ_j (resp. $\boldsymbol{n}_j$) the length (the normal) of a current edge j, $[\![\boldsymbol{\beta}]\!]_{i'}$ the value of the rotation jump at node i' of the current edge. We denote by λ_{UB} the corresponding limit load estimate, highlighting the fact that it yields a rigorous upper bound.

Numerical resolution of the discrete convex minimization problem (4) will be performed using conic programming solvers. We refer to [13] for more details on the implementation of the conic reformulation of (4) and [11, 14] for a discussion on the conic representation of thick plates and thin shells strength criteria and associated support functions.

2.3. A pseudo-upper bound variant

The above formulation (4) still involves the contribution of rotation discontinuities. In the following, we will also consider an even simpler variant which simply ignores this contribution. It can be viewed as a variant of (4) in which only one (instead of two) integration point located at the edge mid-side is used, since we have in this case $[\![\boldsymbol{\beta}]\!]_{\text{mid-side}} = 0$. The corresponding formulation is therefore:

$$\lambda^+ \approx \lambda_{\mathrm{pUB}} = \min_{\boldsymbol{U}} \sum_{e \in \texttt{elements}} \frac{A_e}{3} \sum_{i=1}^{3} \pi_G(\boldsymbol{\chi}_i, \boldsymbol{\gamma}_i) \quad \text{s.t.} \quad \boldsymbol{F}^{\mathrm{T}}\boldsymbol{U} = 1 \tag{5}$$

where we denote by λ_{pUB} the corresponding limit load estimate, highlighting the fact that it is only an approximation (a *pseudo-upper bound*) and not a

strict upper bound.

However, one can hope that the minimizer $\boldsymbol{U}^m$ of (5) will not be far from that of (4). Since $\boldsymbol{U}^m$ is still a candidate for the minimization of (4), we can reconstruct, *a posteriori*, a true upper bound by simply adding the missing contribution:

$$\lambda_{\mathrm{UB2}} = \lambda_{\mathrm{pUB}} + \sum_{j \in \mathtt{edges}} \frac{\ell_j}{2} \sum_{i'=1}^{2} \Pi_G([\![\boldsymbol{\beta}^m]\!]_{i'}, 0; \boldsymbol{n}_j) \tag{6}$$

where $\boldsymbol{\beta}^m$ is the rotation corresponding to the already computed minimizer $\boldsymbol{U}^m$. Obviously, we have that $\lambda_{\mathrm{UB}} \leq \lambda_{\mathrm{UB2}}$ and there is no guarantee that this second upper bound will be of good quality.

3. Extension to shells

We now consider the case of shells using a formulation similar to that of [15] except that it will be simplified to the case of infinitesimal transformations. The shell initial reference configuration consists of piecewise flat portions and $\boldsymbol{\xi}$ in $\mathbb{R}^3$ will denote an initial point on this surface (note that we do not discuss here the geometrical discretization error induced by approaching the shell curved surface by an assembly of planar facets). $(\boldsymbol{e}_1, \boldsymbol{e}_2, \boldsymbol{e}_3)$ will be a reference local frame with $\boldsymbol{e}_3$ the normal to the shell surface, this frame being orthonormal and piecewise constant. A material point $\boldsymbol{X}$ in the shell reference configuration will then be given by:

$$\boldsymbol{X}(\boldsymbol{\xi}, \zeta) = \boldsymbol{\xi} + \zeta \boldsymbol{e}_3 \quad \text{with } \zeta \in [-h/2; h/2] \tag{7}$$

The shell kinematics will be described by its mid-surface displacement $\boldsymbol{u}$ and the infinitesimal rotation vector $\boldsymbol{\theta}$ of its director. The new normal director is $\boldsymbol{a}_3 = \boldsymbol{R}(\boldsymbol{\theta})\boldsymbol{e}_3 = \boldsymbol{e}_3 + \boldsymbol{\theta} \times \boldsymbol{e}_3$ with $\boldsymbol{R}$ the infinitesimal rotation matrix associated with $\boldsymbol{\theta}$. Neglecting any thickness change in the shell kinematics, the material point $\boldsymbol{x}$ in the deformed configuration associated with $\boldsymbol{X}$ will then be given by:

$$\boldsymbol{x} = \boldsymbol{\xi} + \boldsymbol{u}(\boldsymbol{\xi}) + \zeta \boldsymbol{a}_3 = \boldsymbol{\xi} + \boldsymbol{u}(\boldsymbol{\xi}) + \zeta(\boldsymbol{e}_3 + \boldsymbol{\theta}(\boldsymbol{\xi}) \times \boldsymbol{e}_3) \tag{8}$$

Differentiating with respect to $\boldsymbol{X}$, we get:

$$\begin{aligned} d\boldsymbol{x} &= d\boldsymbol{\xi} + \nabla \boldsymbol{u} \cdot d\boldsymbol{\xi} + \zeta(\nabla \boldsymbol{\theta} \cdot d\boldsymbol{\xi}) \times \boldsymbol{e}_3 + d\zeta(\boldsymbol{e}_3 + \boldsymbol{\theta} \times \boldsymbol{e}_3) \\ &= d\boldsymbol{X} + \nabla \boldsymbol{u} \cdot d\boldsymbol{\xi} - \zeta(\boldsymbol{e}_3 \times \nabla \boldsymbol{\theta}) \cdot d\boldsymbol{\xi} - d\zeta(\boldsymbol{e}_3 \times \boldsymbol{\theta}) + \text{ h.o.t.} \end{aligned} \tag{9}$$

where we retained only up to first order terms in $\boldsymbol{u}, \boldsymbol{\theta}$. The 3D deformation gradient is then given by:

$$\boldsymbol{F} = \frac{d\boldsymbol{x}}{d\boldsymbol{X}} = \boldsymbol{I} + \underset{\sim}{\boldsymbol{\nabla}}\boldsymbol{u} - \zeta \boldsymbol{e}_3 \times \underset{\sim}{\boldsymbol{\nabla}}\boldsymbol{\theta} - (\boldsymbol{e}_3 \times \boldsymbol{\theta}) \otimes \boldsymbol{e}_3 \tag{10}$$

where we introduced the in-plane gradient (i.e. the gradient with respect to the shell local tangent plane $(\boldsymbol{e}_1, \boldsymbol{e}_2)$) as follows $\underset{\sim}{\boldsymbol{\nabla}}\boldsymbol{v} = \partial_1 \boldsymbol{v} \otimes \boldsymbol{e}_1 + \partial_2 \boldsymbol{v} \otimes \boldsymbol{e}_2$. More generally, we will use the following notation $\underset{\sim}{\boldsymbol{v}} = v_1 \boldsymbol{e}_1 + v_2 \boldsymbol{e}_2$ to denote the in-plane part of $\boldsymbol{v}$.

The linearized strain tensor is then given by:

$$\boldsymbol{\varepsilon} = \operatorname{sym}\left(\underset{\sim}{\boldsymbol{\nabla}}\boldsymbol{u} - \zeta \boldsymbol{e}_3 \times \underset{\sim}{\boldsymbol{\nabla}}\boldsymbol{\theta} - (\boldsymbol{e}_3 \times \boldsymbol{\theta}) \otimes \boldsymbol{e}_3\right) + \epsilon(\zeta) \boldsymbol{e}_3 \otimes \boldsymbol{e}_3 \tag{11}$$

where we added an incompatible out-of-plane strain $\epsilon(\zeta)$ which will enable to enforce a plane-stress constraint. The 3D strain can be split into its in-plane components $\underset{\approx}{\boldsymbol{\varepsilon}}$, out-of-plane shear components $\boldsymbol{\gamma} = 2\underset{\sim}{\boldsymbol{\varepsilon}}_3$ and out-of-plane transverse components ε_{33}:

$$\underset{\approx}{\boldsymbol{\varepsilon}} = \operatorname{sym}\left(\underset{\sim}{\boldsymbol{\nabla}}\underset{\sim}{\boldsymbol{u}} - \zeta \boldsymbol{e}_3 \times \underset{\sim}{\boldsymbol{\nabla}}\boldsymbol{\theta}\right) = \boldsymbol{\epsilon} - \zeta \boldsymbol{\chi} \tag{12}$$

$$\boldsymbol{\gamma} = \underset{\sim}{\boldsymbol{\nabla}} u_3 - \boldsymbol{e}_3 \times \boldsymbol{\theta} \tag{13}$$

$$\varepsilon_{33} = \epsilon(\zeta) \tag{14}$$

where $\boldsymbol{\epsilon} = \operatorname{sym}(\underset{\sim}{\boldsymbol{\nabla}}\underset{\sim}{\boldsymbol{u}})$ is the membrane strain and $\boldsymbol{\chi} = \operatorname{sym}(\boldsymbol{e}_3 \times \underset{\sim}{\boldsymbol{\nabla}}\boldsymbol{\theta})$ the bending curvature. We see that we recover the definition of the curvature and shear strain of the Reissner-Mindlin plate model.

The internal work of deformation density per shell unit surface is then given by:

$$\begin{aligned} w_{\text{def}} &= \int_{-h/2}^{h/2} \boldsymbol{\sigma} : \boldsymbol{\varepsilon} d\zeta \\ &= \left(\int_{-h/2}^{h/2} \underset{\approx}{\boldsymbol{\sigma}} d\zeta\right) : \boldsymbol{\epsilon} + \left(\int_{-h/2}^{h/2} (-\zeta \underset{\approx}{\boldsymbol{\sigma}}) d\zeta\right) : \boldsymbol{\chi} \\ &\quad + \left(\int_{-h/2}^{h/2} \underset{\sim}{\boldsymbol{\sigma}}_3 d\zeta\right) \cdot \boldsymbol{\gamma} + \int_{-h/2}^{h/2} \sigma_{33} \epsilon(\zeta) d\zeta \\ &= \boldsymbol{N} : \boldsymbol{\epsilon} + \boldsymbol{M} : \boldsymbol{\chi} + \boldsymbol{Q} \cdot \boldsymbol{\gamma} + \int_{-h/2}^{h/2} \sigma_{33} \epsilon(\zeta) d\zeta \end{aligned} \tag{15}$$

where $\boldsymbol{N}$ is the shell membrane tensor, $\boldsymbol{M}$ the bending moment tensor and $\boldsymbol{Q}$ the shear force vector appearing in duality with $\boldsymbol{\epsilon}, \boldsymbol{\chi}, \boldsymbol{\gamma}$ respectively. The out-of-plane stress σ_{33} appears in duality with the out-of-plane strain $\epsilon(\zeta)$. The latter is in fact a purely local variable which can be optimized independently in the upper-bound kinematic approach. This minimization over $\epsilon(\zeta)$ will result in implicitly enforcing a plane stress condition $\sigma_{33} = 0$.

3.1. Shell strength criterion and associated support function

The support function associated with the shell strength criterion can be defined from the local support function of the underlying constitutive material in plane stress condition as follows:

$$\pi_{\text{shell}}(\boldsymbol{\epsilon}, \boldsymbol{\chi}, \boldsymbol{\gamma}) = \sup_{(\boldsymbol{N},\boldsymbol{M},\boldsymbol{Q})\in G_{\text{shell}}} \{\boldsymbol{N} : \boldsymbol{\epsilon} + \boldsymbol{M} : \boldsymbol{\chi} + \boldsymbol{Q} \cdot \boldsymbol{\gamma}\} \tag{16}$$

$$= \int_{-h/2}^{h/2} \sup_{\boldsymbol{\sigma}\in G_{3\text{D}},\sigma_{33}=0} \{\boldsymbol{\sigma} : \boldsymbol{\varepsilon}\} d\zeta \tag{17}$$

$$= \int_{-h/2}^{h/2} \inf_{\epsilon(\zeta)} \pi_{3\text{D}}(\boldsymbol{\varepsilon}) d\zeta \tag{18}$$

Deriving a closed-form expression of π_{shell} is difficult in general. A possible approach is to use a numerical quadrature rule to approximate (18) using the same ideas as in [11]. This approach might however be computationally heavy since it would involve the support function of 3D strength criteria.

In the following, we propose an alternative approximate formulation which might be more simple to implement and easy to compute since it will involve the support function of the corresponding thin shell which involve only a 2D strength criterion, see [11]. Since support functions are positively homogeneous, they satisfy the triangle inequality. An approximation to (18) is therefore obtained as follows:

$$\inf_{\epsilon(\zeta)} \pi_{3\text{D}}(\boldsymbol{\varepsilon}) = \inf_{\epsilon(\zeta)} \pi_{3\text{D}} \left(\underline{\underline{\boldsymbol{\varepsilon}}} + \boldsymbol{\gamma} \overset{s}{\otimes} \boldsymbol{e}_3 + \epsilon(\zeta) \boldsymbol{e}_3 \otimes \boldsymbol{e}_3 \right) \tag{19}$$

$$\leq \inf_{\epsilon(\zeta)} \pi_{3\text{D}} \left(\underline{\underline{\boldsymbol{\varepsilon}}} + \epsilon(\zeta) \boldsymbol{e}_3 \otimes \boldsymbol{e}_3 \right) + \pi_{3D}(\boldsymbol{\gamma} \overset{s}{\otimes} \boldsymbol{e}_3) \tag{20}$$

where the first term can be interpreted as the support function of the pure 2D plane-stress criterion associated with $G_{3\text{D}}$ and the second as the support function of the corresponding pure out-of-plane shear criterion. Both support

functions will be respectively denoted by $\pi_{\text{2D ps}}(\underset{\approx}{\boldsymbol{\varepsilon}})$ and $\pi_{\text{shear}}(\boldsymbol{\gamma})$. Injecting (20) into (18) yields:

$$\pi_{\text{shell}}(\boldsymbol{\epsilon}, \boldsymbol{\chi}, \boldsymbol{\gamma}) \leq \pi_{\text{thin shell}}(\boldsymbol{\epsilon}, \boldsymbol{\chi}) + h\pi_{\text{shear}}(\boldsymbol{\gamma}) \tag{21}$$

$$\text{where} \quad \pi_{\text{thin shell}}(\boldsymbol{\epsilon}, \boldsymbol{\chi}) = \int_{-h/2}^{h/2} \pi_{\text{2D ps}}(\boldsymbol{\epsilon} - \zeta\boldsymbol{\chi}) d\zeta \tag{22}$$

Equation (21) therefore shows that any thick shell support function can be approximated by excess by the sum of a thin shell support function and a pure shear support function. Using classical duality arguments, this upper-bound approximation corresponds to a thick shell strength criterion which neglects any membrane/bending interaction with shearing effects, i.e.:

$$(\boldsymbol{N}, \boldsymbol{M}, \boldsymbol{Q}) \in G_{\text{shell (no interact)}} \Leftrightarrow \begin{cases} (\boldsymbol{N}, \boldsymbol{M}) \in G_{\text{thin shell}} \\ \boldsymbol{Q} \in hG_{\text{shear}} \end{cases} \tag{23}$$

where $G_{\text{thin shell}}$ (resp. G_{shear}) is the thin shell (resp. pure shear) strength criterion whose support function is $\pi_{\text{thin shell}}$ (resp. π_{shear}). This construction generalizes the notion of the no-interaction bending-shear criterion of [10, 14]. Again, regarding the thin shell criterion, any criterion such as those discussed in [11] can be chosen.

Finally, let us point out that a more general approximation of π_{shell} could also be considered by generalizing (21) using a $p-$norm:

$$\pi_{\text{shell}}(\boldsymbol{\epsilon}, \boldsymbol{\chi}, \boldsymbol{\gamma}) \approx ((\pi_{\text{thin shell}}(\boldsymbol{\epsilon}, \boldsymbol{\chi}))^p + (h\pi_{\text{shear}}(\boldsymbol{\gamma}))^p)^{1/p} \tag{24}$$

where the upper-bound status no longer holds, except for $p = 1$ for which we recover (21). Note that for $p = 2$, we recover an elliptic-like interaction akin to [10] in the case of plates.

3.2. Drilling rotation stabilization

A classical problem in shell models involving 6 degrees of freedom (3D rotation) is the absence of any constraint on the drilling rotation $\theta_3 = \boldsymbol{\theta} \cdot \boldsymbol{e}_3$. However, this degree of freedom is necessary to tackle non-smooth junctions between planar shell facets which have a different normal vector. In our implementation, we propose to add an additional resisting work related to the drilling strain ϖ, as commonly done for elastic shells for which a drilling

stiffness is added. The driling strain is obtained from the skew symmetric in-plane component of the transformation gradient:

$$\varpi = \frac{1}{2}(\boldsymbol{a}_1 \cdot \boldsymbol{F} \cdot \boldsymbol{e}_2 - \boldsymbol{e}_2 \cdot \boldsymbol{F}^{\mathrm{T}} \cdot \boldsymbol{a}_1) \tag{25}$$

$$= \frac{1}{2}(\boldsymbol{e}_1 \cdot \boldsymbol{F}^r \cdot \boldsymbol{e}_2 - \boldsymbol{e}_2 \cdot (\boldsymbol{F}^r)^{\mathrm{T}} \cdot \boldsymbol{e}_1) \tag{26}$$

where $\boldsymbol{F}^r = \boldsymbol{R}^{\mathrm{T}}\boldsymbol{F}$ is the back-rotated transformation gradient. Introducing $\boldsymbol{\Theta}$ the skew symmetric matrix associated with $\boldsymbol{\theta}$, we have:

$$\boldsymbol{F}^r = \boldsymbol{R}(-\boldsymbol{\theta})\boldsymbol{F} = (\boldsymbol{I} - \boldsymbol{\Theta})\boldsymbol{F} = \boldsymbol{F} - \boldsymbol{\Theta} + \text{ h.o.t.} \tag{27}$$

where we retained again up to first order terms in $\boldsymbol{u}, \boldsymbol{\theta}$. The in-plane part of $\boldsymbol{F}^r$ is $\underset{\approx}{\boldsymbol{F}}^r = \underset{\approx}{\boldsymbol{I}} + \underset{\sim}{\boldsymbol{\nabla}}\underset{\sim}{\boldsymbol{u}} - \zeta \boldsymbol{e}_3 \times \underset{\sim}{\boldsymbol{\nabla}}\boldsymbol{\theta} - \underset{\approx}{\boldsymbol{\Theta}}$. Computing now $\boldsymbol{e}_1 \cdot \underset{\approx}{\boldsymbol{F}}^r \cdot \boldsymbol{e}_2 - \boldsymbol{e}_2 \cdot (\underset{\approx}{\boldsymbol{F}}^r)^{\mathrm{T}} \cdot \boldsymbol{e}_1$, we see that the drilling strain is affine over the plate thickness. To simplify the formulation, numerical evidence seems to indicate that it is enough to neglect the linear contribution, this amounts to considering an average drilling strain over the shell thickness:

$$\varpi \approx \varpi(\zeta = 0) = \frac{1}{2}(u_{1,2} - u_{2,1}) + \theta_3 \tag{28}$$

If σ_0 denotes a typical value of the material strength (e.g. a tensile strength), we propose to stabilize the drilling rotation by modifying the shell support function as follows:

$$\pi_{\text{shell (stab)}}(\boldsymbol{\epsilon}, \boldsymbol{\chi}, \boldsymbol{\gamma}, \varpi) = \pi_{\text{shell}}(\boldsymbol{\epsilon}, \boldsymbol{\chi}, \boldsymbol{\gamma}) + \sigma_0 h |\varpi| \tag{29}$$

3.3. Numerical implementation

The numerical implementation is exactly the same as for thick plates. We assume a continuous quadratic interpolation for $\boldsymbol{u}$ and a piecewise-linear interpolation for $\boldsymbol{\theta}$ with continuity ensured only at the mid-edges of each element. Although we could also formulate a true upper-bound element as in section 2.2, the subsequent numerical examples only consider the pseudo-upper bound formulation for the sake of simplicity. In the case when no shear interaction is considered (21) for a von Mises material with tensile strength σ_0, the discrete upper-bound limit analysis for shells reads as follows:

$$\begin{aligned} \lambda_{\text{pUB}} = \min_{\boldsymbol{U}} \quad & \sum_{e \in \texttt{elements}} \frac{A_e}{3} \sum_{i=1}^{3} \left(\pi_{\text{thin shell}}(\boldsymbol{\epsilon}_i, \boldsymbol{\chi}_i) + \frac{\sigma_0 h}{\sqrt{3}} \|\boldsymbol{\gamma}_i\|_2 + \sigma_0 h |\varpi_i| \right) \\ \text{s.t.} \quad & \boldsymbol{F}^{\mathrm{T}}\boldsymbol{U} = 1 \end{aligned} \tag{30}$$

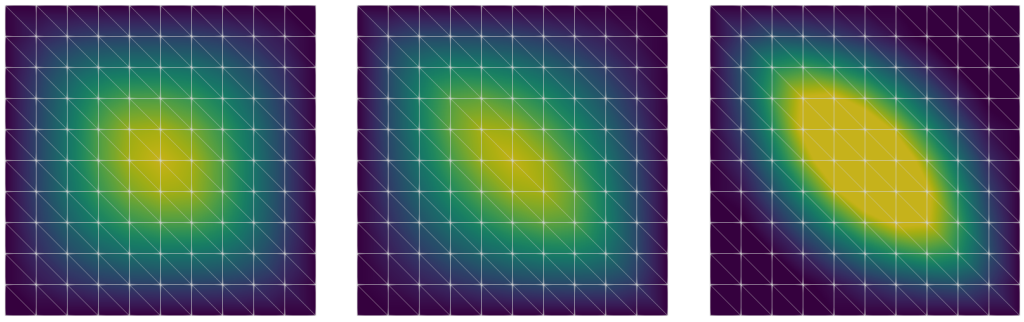

(a) $h/L = 10^{-1}$
$\lambda_k \approx 27.02$

(b) $h/L = 10^{-2}$
$\lambda_k \approx 37.58$

(c) $h/L = 10^{-3}$
$\lambda_k \approx 62.26$

Figure 1: Vertical deflection for the continuous discretization (simple supports)

with notations similar to (4).

4. Illustrative applications

4.1. Square plate problem

A classical benchmark for thick plate limit analysis is the square plate problem of side L made of a von Mises material and subject to a distributed loading of uniform intensity f. For simplicity, we will assume no shear-bending interaction. The limit load factor $\lambda^+ = f^+L^2/M_0$ where $M_0 = \sigma_0 h^2/4$ is known to be $\lambda^+ \approx 25.02$ for simple supports and $\lambda^+ \approx 44.19$ for clamped supports in the thin plate limit [10].

First, let us show visually that the proposed element is free from any shear-locking in the thin plate limit. Figures 1 and 2 represent the vertical deflection isovalues for a continuous discretization and for the present discretization respectively. The mesh is deliberately oriented along a preferential diagonal, since a symmetric criss-crossed mesh is known to be insensitive to shear-locking even if the retained discretization locks in general. As already pointed out in [14], continuous interpolations (quadratic for w and linear for $\boldsymbol{\theta}$) exhibit a strong locking behaviour in the thin plate limit with a clear mesh-orientation dependent solution and an increasing limit load estimate. On the contrary, the present implementation is insensitive to the mesh layout and yields a converging limit load estimate, slightly larger than the reference solution due to the coarse discretization.

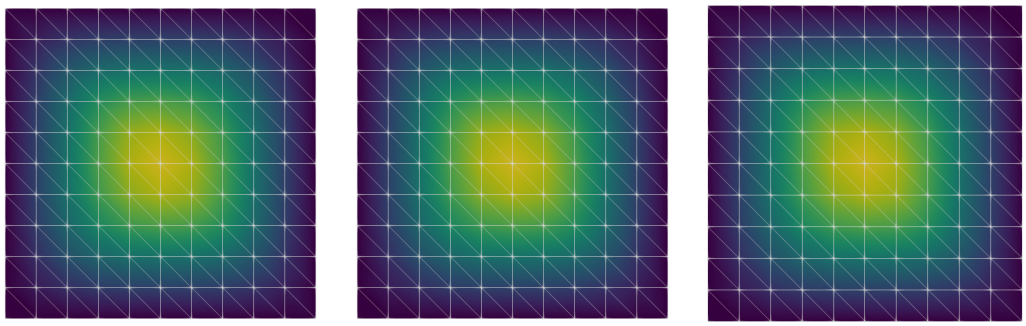

(a) $h/L = 10^{-1}$
$\lambda_k \approx 25.46$

(b) $h/L = 10^{-2}$
$\lambda_k \approx 25.47$

(c) $h/L = 10^{-3}$
$\lambda_k \approx 25.47$

Figure 2: Vertical deflection for the proposed discretization (simple supports)

More quantitatively, mesh convergence with respect to the number of degrees of freedom is represented in Figure 3. An unstructured mesh has been used for a thickness ratio $h/L = 0.01$. Results have been presented for the pseudo-upper bound estimate λ_{pUB} of (5), the corresponding post-processed upper-bound λ_{UB2} of (6), the true upper-bound λ_{UB} of (4) as well as the upper-bound obtained with fully discontinuous elements λ_{DG} of [14].

One can first observe that the pseudo-upper bound is of extremely good quality and seems to converge from above. It is even more accurate than the fully discontinuous interpolation which has a much richer interpolation. The true upper-bound λ_{UB} is also of good quality and becomes competitive compared to λ_{DG} when increasing the problem size. The reconstructed upper-bound is, as expected moderately larger than λ_{UB}.

The previous results have been presented against the total number of mechanical degrees of freedom w and $\boldsymbol{\theta}$. However, even with similar number of dofs, formulations including discontinuity terms are slightly harder to optimize due to the presence of additional auxiliary variables and, sometimes, a larger number of iterations required for convergence. Thus, the previous results are even more favourable for the proposed discretization when considering the total computing time.

4.2. L-plate problem

We revisit the L-plate problem already investigated in previous references [10, 14, 29] with uniformly distributed loading f and simple supports on two opposite sides (see Figure 4a). For this computation, we used the ellipsoid

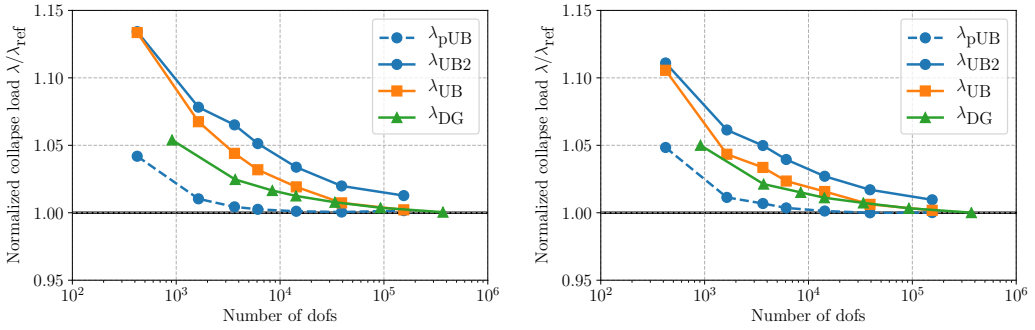

(a) simple supports

(b) clamped supports

Figure 3: Mesh convergence with respect to the number of degrees of freedom

criterion of bending/shear interaction as described in [10, 14]. Computations have again been compared against a fully discontinuous element (λ_{DG}) and the lower-bound equilibrium element (λ_{LB}) presented in [10].

The evolution of the computed ultimate load $\lambda^+ = f^+L^2/M_0$ as a function of the plate slenderness ratio L/h has been represented in Figure 4b. Clearly, the present true upper bound element performs very well for all slenderness ratios. On the contrary, the *a posteriori* reconstructed upper bound λ_{UB2} does not yield satisfying results in the present case. This may be attributed to the fact that discontinuities in the solution are much more important in this example, both in the bending and in the shear-dominated regimes, than for the previous square plate example. However, as before, the pseudo-upper bound λ_{pUB} is again of very good quality, even better than λ_{UB}. We can remark that for moderately thick plates, the computed estimate is slightly lower than the lower bound of [10].

4.3. Collapse of a cylindrical thin shell

To validate the implementation for shells, the problem of a cylindrical shell of length $2L$, radius R and thickness $h = 0.01R$, clamped at both extremities and loaded by a self-weight uniform vertical loading $\boldsymbol{f} = -q\boldsymbol{e}_z$ is considered (see Figure 5a and [11]). The shape of the collapse mechanism varies depending on the cylinder slenderness $2L/R$. For sufficiently long cylinders, the computed limit load q^+ is well described by the one obtained when representing the cylinder as a 1D beam $q^+_{\text{beam}} = \frac{32}{\pi}\sigma_0 h \left(\frac{R}{2L}\right)^2$. To

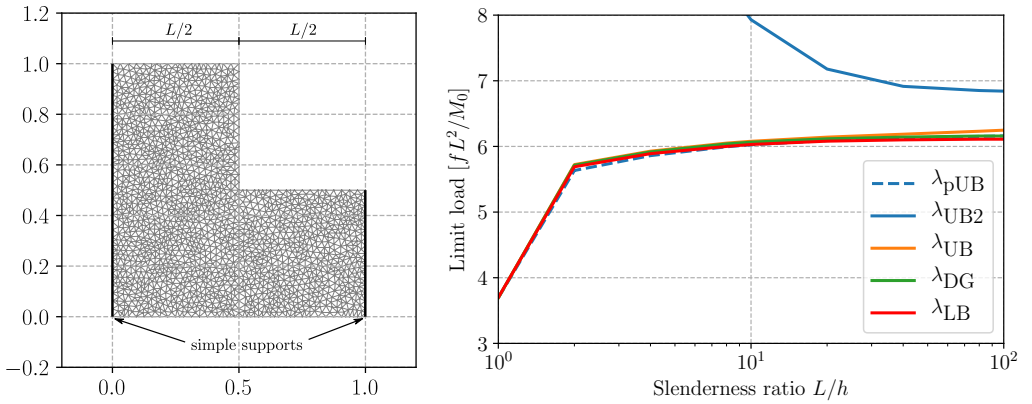

(a) Mesh and boundary conditions

(b) Normalized collapse load $\lambda^+ = f^+ L^2/M_0$ as a function of the plate slenderness: lower-bound results λ_{LB} correspond to those of [10]

Figure 4: L-plate problem under uniform loading

compare our results with those of [11], we also used the numerical quadrature approach to compute $\pi_{\text{thin shell}}(\boldsymbol{\epsilon}, \boldsymbol{\chi})$ in the thickness direction using 5 integration points.

Results are represented in Figure 5b and show that the computed pseudo-upper bound is very close to the true upper bound of [11] using the same mesh. We also verified that increasing the amplitude of the drilling rotation stabilization term in (30) did not influence the results.

4.4. Sequential limit analysis on a sphere-cap shell

Finally, we consider a sequential limit analysis problem in which the structure geometry is updated step-by-step using the collapse mechanism obtained from the solution of the upper-bound approach. This heuristic method has been first proposed in [50] to assess the post-collapse of structures in a simplified manner. We also refer to [31] for a recent and thorough discussion on its range of applicability. Some applications of sequential limit analysis on shell structures can also be found in [18, 19, 43].

A spherical cap shell of radius R, thickness h and opening angle α is subjected to a uniformly distributed external radial pressure p and is simply supported on its boundary (see Figure 6a). For numerical applications, we chose $R = 10$ m, $h = 0.1$ m and $\alpha = 32°$. In the sequential limit analysis process, we monitor the evolution of the limit load as a function of the shell

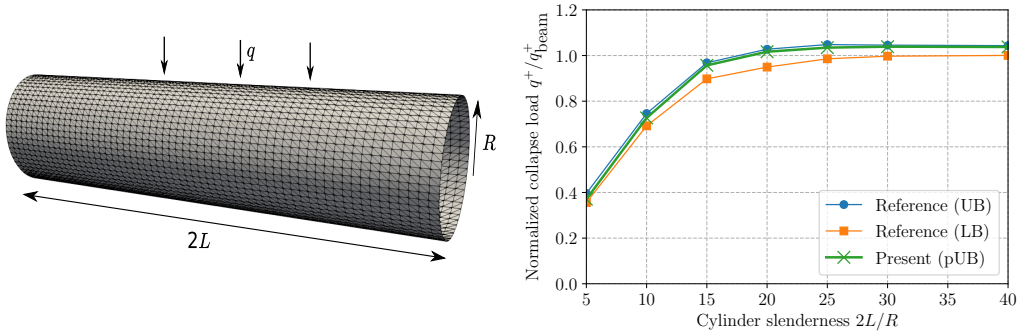

(a) Geometry and loading, fixed supports at both extremities

(b) Limit load as a function of the shell slenderness: reference solutions are those of [11]

Figure 5: A cylindrical thin shell problem

downwards vertical displacement of its apex. We renormalize the obtained collapse mechanism to apply a uniform displacement increment of 1 cm. Results have been represented on Figure 6b where it can first be noted that initially, the limit load is equal to the theoretical value of $p^+ = 2\sigma_0 h/R$ (see [11]). The limit load then rapidly decreases when updating the geometry with the computed mechanism, a strong drop can be observed which corresponds to the transition towards a configuration with an inverted curvature near the shell central region. The evolution of the shell geometry during the sequential limit analysis procedure has been represented in Figure 6c.

5. Conclusions

In this contribution, we investigated the use of a new discretization strategy for the limit analysis of Reissner-Mindlin plates. The use of a continuous P^2 Lagrange discretization for the deflection and of a non-conforming Crouzeix-Raviart element (linear with continuity at mid-edges only) for the rotation avoids any shear-locking issue in the thin plate limit. The proposed choice has several advantages:

- it avoids the need of cumbersome techniques to resolve the shear-locking issue which usually destroy the upper bound status of the result;
- it is simpler to implement and results in less degrees of freedom than fully discontinuous approaches;

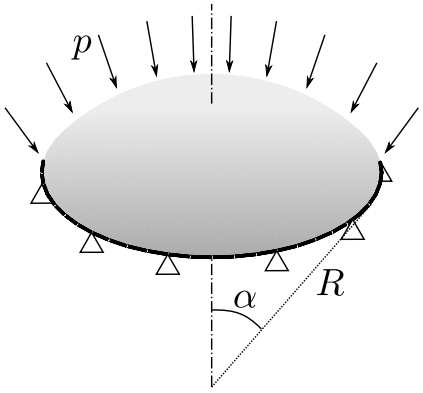

(a) Geometry

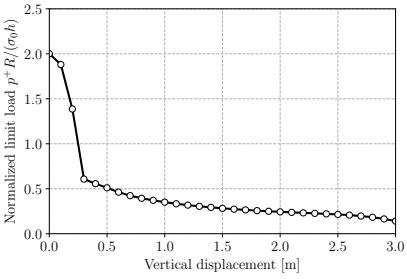

(b) Evolution of the limit load with downwards vertical deflection

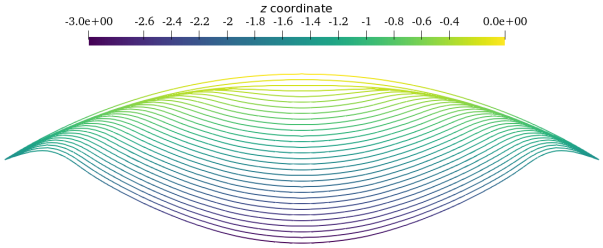

(c) Evolution of the shell geometry during sequential limit analysis

Figure 6: Sequential limit analysis on a sphere-cap shell

- a simple pseudo-upper bound can be obtained by neglecting the contribution of rotation discontinuities;
- numerical examples show that this estimate is particularly accurate and tend to converge from above.

Finally, we also extend the proposed element to the case of thick shells. In this respect, we discussed the formulation of strength criteria for thick shells, which has never been previously done to our knowledge. The proposed implementation for shells also remains simple, one must only include a drilling rotation penalty to account for this supplementary degree of freedom compared to the case of plates.

Future works might involve extending this discretization strategy to multilayered plates or shells with proper accounting of interfacial effects between successive layers. Taking into account geometry changes is obviously extremely important for such structures. Although sequential limit analysis might be a simple approach as illustrated previously, its range of application is still debatable and should deserve more extensive work for applications on shell structures.

References

[1] Alnæs, M.S., Blechta, J., Hake, J., Johansson, A., Kehlet, B., Logg, A., Richardson, C., Ring, J., Rognes, M.E., Wells, G.N., 2015. The fenics project version 1.5. Archive of Numerical Software 3. doi:10.11588/ans.2015.100.20553.

[2] Anderheggen, E., Knöpfel, H., 1972. Finite element limit analysis using linear programming. International Journal of Solids and Structures 8, 1413–1431.

[3] Arnold, D.N., Falk, R.S., 1989. A uniformly accurate finite element method for the Reissner–Mindlin plate. SIAM Journal on Numerical Analysis 26, 1276–1290.

[4] Bisbos, C., Papaioannou, G., 2006. Shakedown analysis of fem-discretized steel shell structures under the ilyushin yield criterion. Nonsmooth/Nonconvex Mechanics with Applications in Engineering, II. NN-MAE2006, In Memoriam of Professor PD Panagiotopoulos, Editions ZITI, Thessaloniki , 197–204.

[5] Bisbos, C., Pardalos, P., 2007. Second-order cone and semidefinite representations of material failure criteria. Journal of Optimization Theory and Applications 134, 275–301.

[6] Bleyer, J., 2018. Numerical Tours of Computational Mechanics with FEniCS. doi:10.5281/zenodo.1287832.

[7] Bleyer, J., 2020a. Automating the formulation and resolution of convex variational problems: Applications from image processing to computational mechanics. ACM Transactions on Mathematical Software 3, 27. URL: https://doi.org/10.1145/3393881, doi:10.1145/3393881.

[8] Bleyer, J., 2020b. fenics-optim – Convex optimization interface in FEniCS. URL: https://doi.org/10.5281/zenodo.3778848, doi:10.5281/zenodo.3778848.

[9] Bleyer, J., de Buhan, P., 2013. On the performance of non-conforming finite elements for the upper bound limit analysis of plates. International Journal for Numerical Methods in Engineering 94, 308–330.

[10] Bleyer, J., de Buhan, P., 2014. Lower bound static approach for the yield design of thick plates. International Journal for Numerical Methods in Engineering 100, 814–833.

[11] Bleyer, J., de Buhan, P., 2016. A numerical approach to the yield strength of shell structures. European Journal of Mechanics-A/Solids 59, 178–194.

[12] Bleyer, J., Carlier, G., Duval, V., Mirebeau, J.M., Peyré, G., 2016. A γ-convergence result for the upper bound limit analysis of plates. ESAIM: Mathematical Modelling and Numerical Analysis 50, 215–235.

[13] Bleyer, J., Hassen, G., 2021. Automated formulation and resolution of limit analysis problems. Computers & Structures 243, 106341. URL: http://www.sciencedirect.com/science/article/pii/S0045794920301449, doi:https://doi.org/10.1016/j.compstruc.2020.106341.

[14] Bleyer, J., Le, C.V., de Buhan, P., 2015. Locking-free discontinuous finite elements for the upper bound yield design of thick plates. International Journal for Numerical Methods in Engineering 103, 894–913.

[15] Campello, E., Pimenta, P., Wriggers, P., 2003. A triangular finite shell element based on a fully nonlinear shell formulation. Computational Mechanics 31, 505–518.

[16] Capsoni, A., Corradi, L., 1999. Limit analysis of plates- a finite element formulation. Structural Engineering and Mechanics 8, 325–341.

[17] Casciaro, R., Cascini, L., 1982. A mixed formulation and mixed finite elements for limit analysis. International Journal for Numerical Methods in Engineering 18, 211–243.

[18] Corradi, L., Panzeri, N., 2003. Post-collapse analysis of plates and shells based on a rigid–plastic version of the tric element. Computer methods in applied mechanics and engineering 192, 3747–3775.

[19] Corradi, L., Panzeri, N., 2004. A triangular finite element for sequential limit analysis of shells. Advances in Engineering software 35, 633–643.

[20] Crouzeix, M., Raviart, P.A., 1973. Conforming and nonconforming finite element methods for solving the stationary stokes equations i. ESAIM: Mathematical Modelling and Numerical Analysis-Modélisation Mathématique et Analyse Numérique 7, 33–75.

[21] Garcea, G., Leonetti, L., 2011. A unified mathematical programming formulation of strain driven and interior point algorithms for shakedown and limit analysis. International Journal for Numerical Methods in Engineering 88, 1085–1111.

[22] Garcea, G., Leonetti, L., 2013. Decomposition methods and strain driven algorithms for limit and shakedown analysis, in: Limit State of Materials and Structures. Springer, pp. 19–43.

[23] Hale, J.S., Brunetti, M., Bordas, S.P., Maurini, C., 2018. Simple and extensible plate and shell finite element models through automatic code generation tools. Computers & Structures 209, 163–181.

[24] Hill, R., 1950. The mathematical theory of plasticity. Clarendon Press, Oxford.

[25] Hodge Jr, P.G., Belytschko, T., 1968. Numerical methods for the limit analysis of plates. Journal of Applied Mechanics 35, 796.

[26] Karmarkar, N., 1984. A new polynomial-time algorithm for linear programming, in: Proceedings of the sixteenth annual ACM symposium on Theory of computing, ACM. pp. 302–311.

[27] Krabbenhoft, K., Damkilde, L., 2002. Lower bound limit analysis of slabs with nonlinear yield criteria. Computers & structures 80, 2043–2057.

[28] Krabbenhoft, K., Lyamin, A.V., Hjiaj, M., Sloan, S.W., 2005. A new discontinuous upper bound limit analysis formulation. International Journal for Numerical Methods in Engineering 63, 1069–1088.

[29] Le, C.V., 2013. A stabilized discrete shear gap finite element for adaptive limit analysis of Mindlin–Reissner plates. International Journal for Numerical Methods in Engineering 96, 231–246.

[30] Le, C.V., Nguyen-Xuan, H., Nguyen-Dang, H., 2010. Upper and lower bound limit analysis of plates using fem and second-order cone programming. Computers & Structures 88, 65–73.

[31] Leblond, J.B., Kondo, D., Morin, L., Remmal, A., 2018. Classical and sequential limit analysis revisited. Comptes Rendus Mécanique 346, 336–349.

[32] Lee, S., Wong, S., 1982. Mixed formulation finite elements for mindlin theory plate bending. International Journal for Numerical Methods in Engineering 18, 1297–1311.

[33] Logg, A., Mardal, K.A., Wells, G., 2012. Automated solution of differential equations by the finite element method: The FEniCS book. volume 84. Springer Science & Business Media.

[34] Lysmer, J., 1970. Limit analysis of plane problems in soil mechanics. Journal of Soil Mechanics & Foundations Div 96, 1311–1334.

[35] Makrodimopoulos, A., 2010. Remarks on some properties of conic yield restrictions in limit analysis. International Journal for Numerical Methods in Biomedical Engineering 26, 1449–1461.

[36] Makrodimopoulos, A., Martin, C., 2007. Upper bound limit analysis using simplex strain elements and second-order cone programming. International journal for numerical and analytical methods in geomechanics 31, 835–865.

[37] Makrodimopoulos, A., Martin, C., 2008. Upper bound limit analysis using discontinuous quadratic displacement fields. Communications in Numerical Methods in Engineering 24, 911–927.

[38] Martin, C.M., Makrodimopoulos, A., 2008. Finite-element limit analysis of Mohr–Coulomb materials in 3d using semidefinite programming. Journal of Engineering Mechanics 134, 339–347.

[39] Martins, R.R., Zouain, N., Borges, L., de Souza Neto, E.A., 2014. A continuum-based mixed shell element for shakedown analysis. European Journal of Mechanics-A/Solids 47, 156–173.

[40] MOSEK ApS, ., 2018. The MOSEK optimization API for Python 8.1.0. URL: `http://docs.mosek.com/8.1/pythonapi/index.htm`.

[41] Nesterov, Y., Nemirovskii, A., Ye, Y., 1994. Interior-point polynomial algorithms in convex programming. volume 13. SIAM.

[42] Pastor, J., Turgeman, S., 1976. Mise en œuvre numérique des méthodes de l'analyse limite pour les matériaux de von mises et de coulomb standards en déformation plane. Mechanics Research Communications 3, 469–474.

[43] Raithatha, A., Duncan, S., 2009. Rigid plastic model of incremental sheet deformation using second-order cone programming. International journal for numerical methods in engineering 78, 955–979.

[44] Salençon, J., 1983. Calcul à la rupture et analyse limite. Presses de l'Ecole Nationale des Ponts et Chaussées.

[45] Salençon, J., 2013. Yield Design. London, Hoboken : ISTE Ltd., John Wiley & Sons, Inc.

[46] Simo, J.C., Rifai, M., 1990. A class of mixed assumed strain methods and the method of incompatible modes. International journal for numerical methods in engineering 29, 1595–1638.

[47] Sloan, S.W., 1988. Lower bound limit analysis using finite elements and linear programming. International Journal for Numerical and Analytical Methods in Geomechanics 12, 61–77.

[48] Sloan, S.W., Kleeman, P.W., 1995. Upper bound limit analysis using discontinuous velocity fields. Computer Methods in Applied Mechanics and Engineering 127, 293 – 314.

[49] Tran, T.N., Kreißig, R., Vu, D.K., Staat, M., 2008. Upper bound limit and shakedown analysis of shells using the exact Ilyushin yield surface. Computers & Structures 86, 1683–1695.

[50] Yang, W.H., 1993. Large deformation of structures by sequential limit analysis. International journal of solids and structures 30, 1001–1013.

[51] Zienkiewicz, O., Taylor, R., Too, J., 1971. Reduced integration technique in general analysis of plates and shells. International Journal for Numerical Methods in Engineering 3, 275–290.